



Research Article

Effect of Laser Heating on Partial Decomposition of $\text{Bi}_{12}\text{SiO}_{20}$ (BSO) Single Crystal: Raman Study

Nebojsa Romcevic ¹, Branka Hadzic,¹ Marija Prekajski Đorđević,² Peda Mihailovic,³ Milica Curcic,¹ Jelena Trajic,¹ Jelena Mitric,¹ and Maja Romcevic ¹

¹Institute of Physics Belgrade, University of Belgrade, Belgrade 11080, Serbia

²Vinca Institute of Nuclear Sciences, University of Belgrade, Belgrade 11000, Serbia

³School of Electrical Engineering, University of Belgrade, Belgrade 11000, Serbia

Correspondence should be addressed to Nebojsa Romcevic; romcevi@ipb.ac.rs

Received 2 March 2023; Revised 17 April 2023; Accepted 28 April 2023; Published 4 May 2023

Academic Editor: Emiliano Bonera

Copyright © 2023 Nebojsa Romcevic et al. This is an open access article distributed under the Creative Commons Attribution License, which permits unrestricted use, distribution, and reproduction in any medium, provided the original work is properly cited.

The effect of laser (532 nm line of Verdi G) heating during the Raman measurements, on partial decomposition of $\text{Bi}_{12}\text{SiO}_{20}$ single crystal, was addressed in this study. The degree of decomposition directly depends on the power density and duration of the laser treatment, which are registered by the phonon Raman spectra. After laser treatment, AFM measurements register additional small spherical islands on the surface. Analysis performed on irradiated and unirradiated samples showed significant changes in transmission spectra, X-ray diffraction (XRD) pattern, Verdet constant, magneto-optical property, and absorption coefficient. The material obtained after laser irradiation can be described as specific nanocomposite consisting of bismuth oxide and silicon oxide-based nano-objects (dimensions below 15 nm in diameter), which are arranged in a matrix of $\text{Bi}_{12}\text{SiO}_{20}$.

1. Introduction

Sillenite crystals belong to the $\text{Bi}_{12}\text{MO}_{20}$ group (where $M = \text{Si}, \text{Ge}, \text{and Ti}$) compounds, that have a body-centered cubic crystalline structure with the space group $I23$ [1]. Crystal $\text{Bi}_{12}\text{SiO}_{20}$ has parameters $a = 1.01067 \text{ nm}$, $Z = 2$ (two identical motives in the unit cell). The density functional theory calculations presented bandgap energy of $\text{Bi}_{12}\text{SiO}_{20}$ as 3.43 eV [2]. Experimentally determined values are lower [3]. These optically active crystals can exhibit many strong effects such as magneto-optical, photo-induced, and electro-optical effects. Also, they possess numerous interesting properties, such as high values of piezo-electric, dielectric and elasto-optic constants, as well as high dark electric resistance [1]. These crystals, usually as bulk crystals, have widespread applications as active elements in many devices, such as optical limiting, holography, spatial light modulation, optical phase conjugation, optical memories fiber optic sensors, and Pockels cells [4–6].

Lasers have great applications in material processing [7] and their role is only getting more expanded. The surface of a single crystal can be laser treated [8] whereby a thin surface layer of the material is transformed when it interacts with the laser beam. This process is strictly controlled with the laser beam wavelength and power, its duty cycle, and repetition rate. The final result of how material is modified depends on a sample, since all materials have unique properties that dictate how they will interact with the laser radiation [9, 10].

Raman spectroscopy is an established technique to measure local material properties [11]. As such, it is very suitable for research related to the surface of the sample. However, since it uses a laser for excitation, structural changes may occur on the surface of the sample caused by local heating. In some cases, these modifications can lead to the decomposition of the sample, which results in a changed Raman signal [12, 13]. Changes in the spectrum can be in the position and half-width of phonon lines on the spectrum of

the starting material, as well as lead to the appearance of new lines caused by permanent modifications in the sample [14, 15].

In our previous paper [16], we registered the decomposition of $\text{Bi}_{12}\text{SiO}_{20}$ (BSO) single crystal due to femtosecond laser irradiation. By far-infrared spectroscopy and AFM measurements, the existence of bismuth oxide nano-objects on the surface of the sample was registered. XRD could not register these changes. Also, it was not possible to establish control parameters between the formed nano-objects and the conditions of the experiment because the sample was treated in advance. Also, for the same reason, it was not possible to determine the exact phase composition of nano-objects.

The aim of this work is to continue the investigation of the influence of locally induced heating, with an increase in the power density of the semiconductor laser during Raman measurements, on the $\text{Bi}_{12}\text{SiO}_{20}$ single crystal. In this way, direct results related to the current state of $\text{Bi}_{12}\text{SiO}_{20}$ decomposition will be provided, as well as parameters that can control that process. Complementary techniques such as X-ray diffraction (XRD), atomic force microscopy (AFM), UV-Vis transmission, and magneto-optical measurements will be used in the characterization of the obtained materials.

2. Materials and Methods

The Czochralski technique was applied to grow $\text{Bi}_{12}\text{SiO}_{20}$ single crystal, which is described in more detail in Ref. [16]. In short, MSR 2 crystal puller controlled by a Eurotherm was used. A platinum crucible was used to contain the melt, which was placed in an alumina vessel on zircon-oxide wool. Crystal growth was occurred in an air. Bi_2O_3 and SiO_2 were used for the synthesis of crystals. Starting materials were mixed in 6:1 stoichiometric ratio. Optimal pull rate was chosen in the range 5-6 mm/h. Equations of the melt hydrodynamics were used to calculate the critical crystal diameter, $d_c = 10$ mm, and critical rotation, $\omega_c = 20$ rpm. The crucible was not rotating during crystal growth. The crystal boule was cooled at $\sim 50^\circ\text{C}/\text{h}$ down to a room temperature, after the crystal growth. Crystals grew in [111] direction, without core being observed. Finally, crystals were cut and polished.

Polished crystal samples were treated using Verdi G optical pumped semiconductor laser with a 532 nm wavelength with different irradiation times during Raman experiment.

Atomic Force Microscopy (AFM) was used to determine topography of the samples with NTEGRA prima from NT-MDT.

The X-ray diffraction (XRD) data was measured using an X-ray diffractometer (XRD) Rigaku Ultima IV, Japan. The PDXL2 v2.0.3.0 software, with reference to the diffraction patterns available in the International Center for Diffraction Data (ICDD) [17], was used for phase identification and data analysis.

The UV-Vis transmission spectra were collected in the 200–900 nm range using a Perkin-Elmer Lambda 4B UV-Vis spectrophotometer.

Raman spectra of prepared samples were obtained using backscattering configuration of Jobin Yvon T64000 spectrometer equipped with nitrogen cooled CCD detector. The spectra were recorded in the spectral range 80–650 cm^{-1} at room temperature using a 532 nm Verdi G optical pumped semiconductor laser line.

Parameters such as Faraday rotation, bulk absorption, and optical activity were measured at 632.8 nm using a He-Ne laser. This was obtained by an orthogonal polarization detection polarimetric method [18].

3. Results

3.1. Raman Spectroscopy. Raman spectra of $\text{Bi}_{12}\text{SiO}_{20}$ (BSO) single crystal, nanocrystalline powders, and thin films have been measured and analyzed in the past [19–22]. Identification of the observed peaks was performed on the basis of the factor group analysis for the SiO_4 tetrahedra, OBi_3 , and Bi_3O_4 structural fragments. The Raman spectrum of the our $\text{Bi}_{12}\text{SiO}_{20}$ single crystal is shown in Figure 1(a). The spectrum was recorded with a laser power density of 0.1 $\text{mW}/\mu\text{m}^2$ and the measurement time of 5 s, which did not cause structural changes in the sample. The spectrum of $\text{Bi}_{12}\text{SiO}_{20}$ exhibits intense modes at about 87, 97, 104, 128, 144, 167, 176, 204, 269, 322, and 536 cm^{-1} . As expected, our spectrum from Figure 1(a) is identical to the literature data [19–22].

Raman spectra of a $\text{Bi}_{12}\text{SiO}_{20}$ single crystal recorded consecutively at different laser powers (0.5–2 $\text{mW}/\mu\text{m}^2$) and the recording time of each measurement of 30 s, at the same place on the sample are shown in Figure 1(b). The intensity of the peaks registered in Figure 1(a) increases with increasing laser power. In addition, starting with the laser power of 0.7 $\text{mW}/\mu\text{m}^2$ additional structures were seen on the spectra at about 122, 235, 456, and 487 cm^{-1} . They are significantly weaker than already registered phonons, but their intensity also increases with increasing laser power. The result was checked with the same laser power, but with a measurement times of 1 s and 60 s. Raman spectra of $\text{Bi}_{12}\text{SiO}_{20}$ single crystal recorded at laser power density of 1.5 $\text{mW}/\mu\text{m}^2$ and different recording times at different locations on the sample are shown in Figure 1(c). A very short 1 s measurement excites a spectrum similar to that in Figure 1(a). An increase in recording time leads to the same effect registered in Figure 1(b). To explain the registered effect, it was necessary to do additional experiments.

3.2. AFM. Figure 2 shows the results of AFM measurements of the $\text{Bi}_{12}\text{SiO}_{20}$ single crystal and the same sample after the Raman measurements (shown in Figure 1(c)). In Figure 2(a), we can clearly see that the surface of the untreated sample is quite smooth with no visible cracks, and only traces of mechanical polishing can be seen. Figures 2(b) and 2(c) show the surface of the sample after laser treatment of 1.5 $\text{mW}/\mu\text{m}^2$, according to the procedure described in Section 3.1, with two different time lengths of each measurement (30 s and 60 s), respectively. Nano-objects, small white dots in the images, with a diameter of about 11 nm (Figure 2(b)) and 15 nm (Figure 2(c)) were observed on both

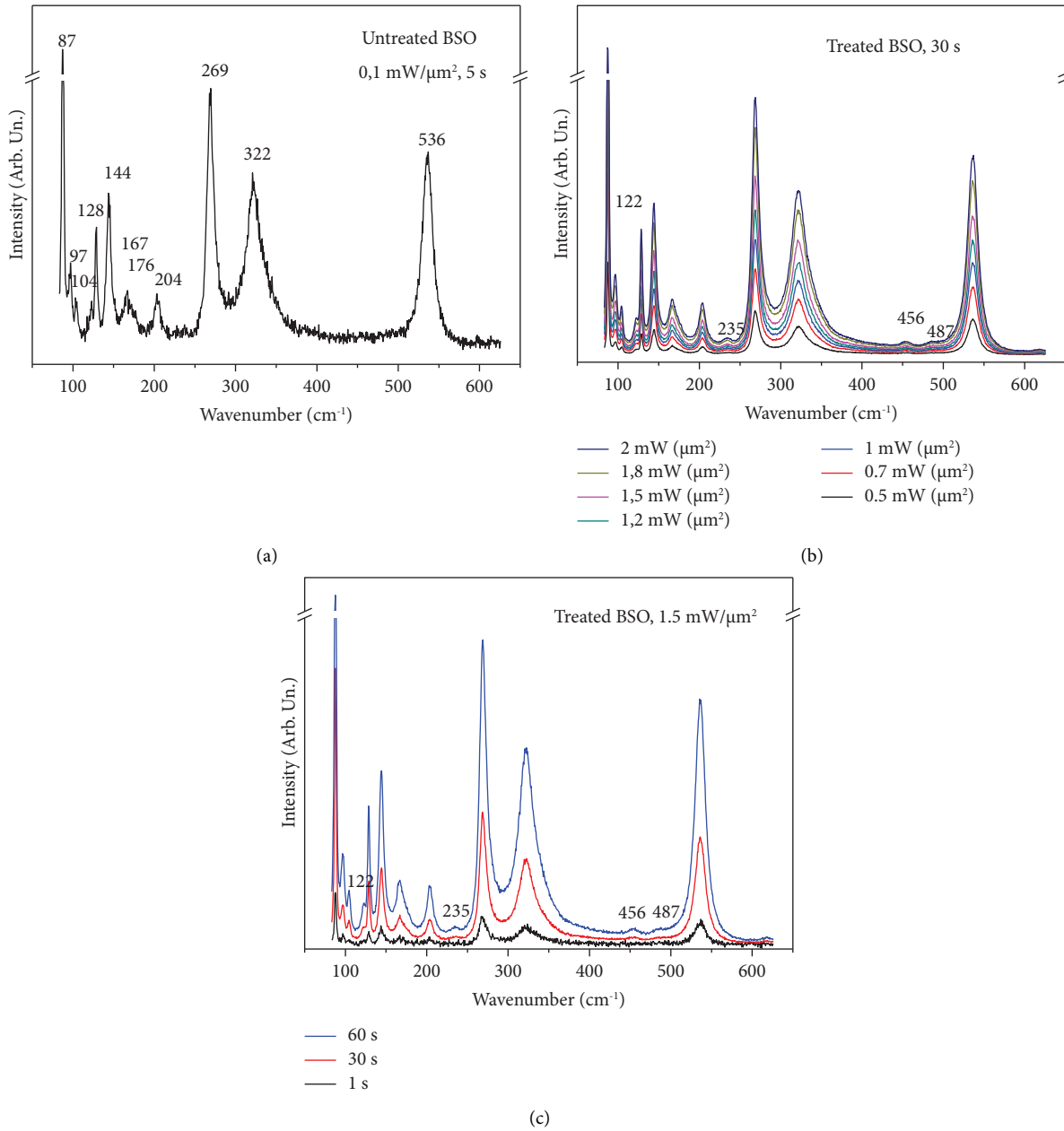


FIGURE 1: (a) Raman spectrum of the $\text{Bi}_{12}\text{SiO}_{20}$ single crystal. (b) Raman spectra of $\text{Bi}_{12}\text{SiO}_{20}$ single crystal recorded consecutively at different laser powers at the same location on the sample. (c) Raman spectra of $\text{Bi}_{12}\text{SiO}_{20}$ single crystal recorded with laser power of $1.5 \text{ mW}/\mu\text{m}^2$ and different recording times at different locations on the sample.

images. In Figure 2(c) we see that the density of nano-objects is significantly higher than that registered in Figure 2(b).

3.3. XRD Measurements. The XRD patterns of prepared BSO single crystal and BSO laser treated ($1.5 \text{ mW}/\mu\text{m}^2$, 60 s) are presented in Figure 3. From the XRD pattern of untreated BSO single crystal (the bottom spectrum) it is clearly seen that all peaks correspond to $\text{Bi}_{12}\text{SiO}_{20}$. Results show that only selenite ($\text{Bi}_{12}\text{SiO}_{20}$) phase is present, which corresponds to the JCPDF Card No. 37-0485. When compared to laser treated BSO single crystal (upper spectrum), except selenite

peaks are observed. These peaks correspond to: Bi_4O_7 (JCPDF Card No. 01-074-2352), Bi_2O_3 (00-057-0400, 00-051-1161, and 01-079-6679), and SiO_2 (01-071-5334) phases. All additional phases are marked with different symbols in Figure 3.

XRD results clearly and unequivocally show the influence of locally induced heating with laser power on $\text{Bi}_{12}\text{SiO}_{20}$ single crystal as the separation of new phases in the form of different Bi_4O_7 , Bi_2O_3 , and SiO_2 . These results explain the appearance of additional structures seen on the Raman spectra whose intensity increases with increasing

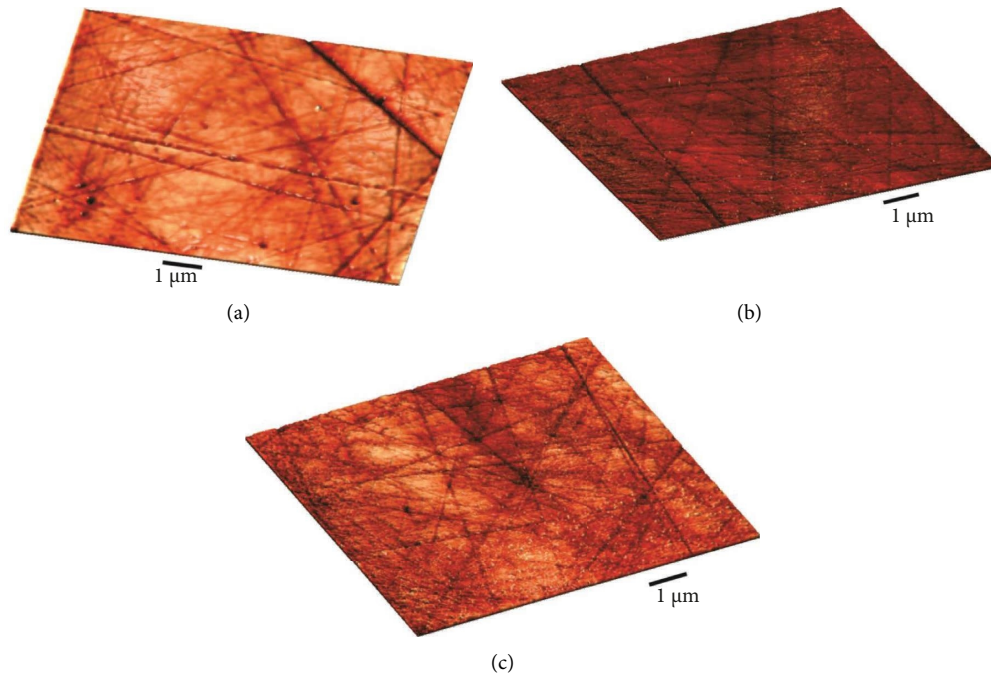


FIGURE 2: AFM results of: untreated $\text{Bi}_{12}\text{SiO}_{20}$ single crystal (a); laser treated $\text{Bi}_{12}\text{SiO}_{20}$ sample $P = 1.5 \text{ mW}/\mu\text{m}^2$: 30 s (b); and 60 s (c).

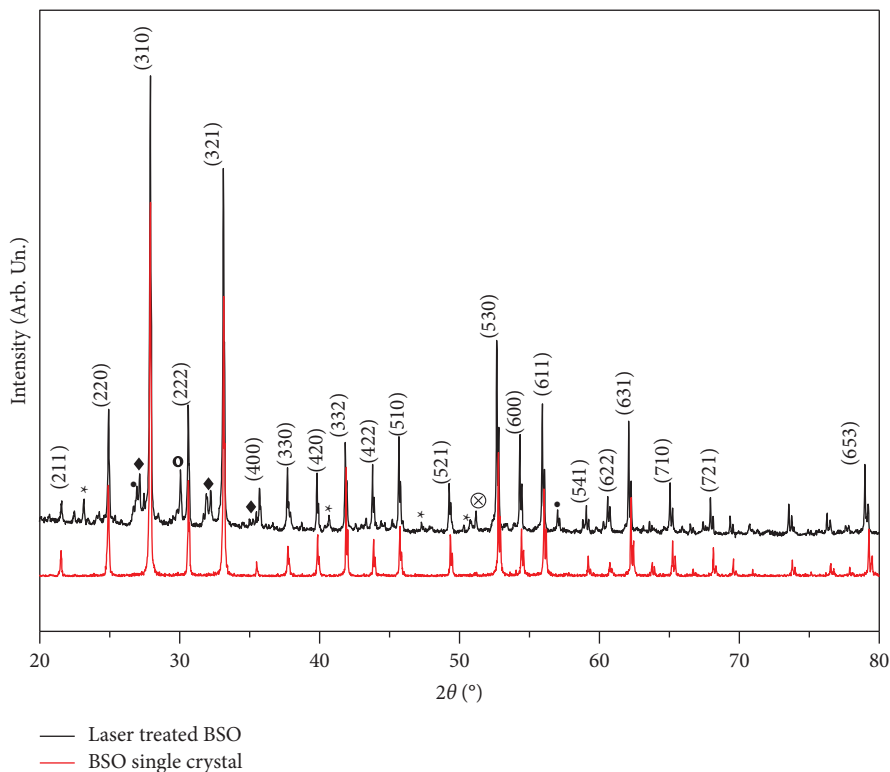


FIGURE 3: X-ray diffraction results of untreated and laser treated BSO single crystal, peaks of $\text{Bi}_{12}\text{SiO}_{20}$ phase marked with hkl , * Bi_4O_7 (JCPDF Card No. 01-074-2352), ◆ SiO_2 (01-071-5334), ○ Bi_2O_3 (00-057-0400), ● Bi_2O_3 (00-051-1161), and ⊗ Bi_2O_3 (01-079-6679).

laser power and measurement time. The appearances of secondary phases also explain the phenomenon of additional small white dots (nano-objects) in the AFM images of laser-treated samples.

3.4. UV-Vis Spectroscopy. In Figure 4(a) the results of transmission measurements of BSO samples in the UV-VIS region are presented. It is noticeable that for the laser-treated sample in the area of wavelength above 550 nm, the

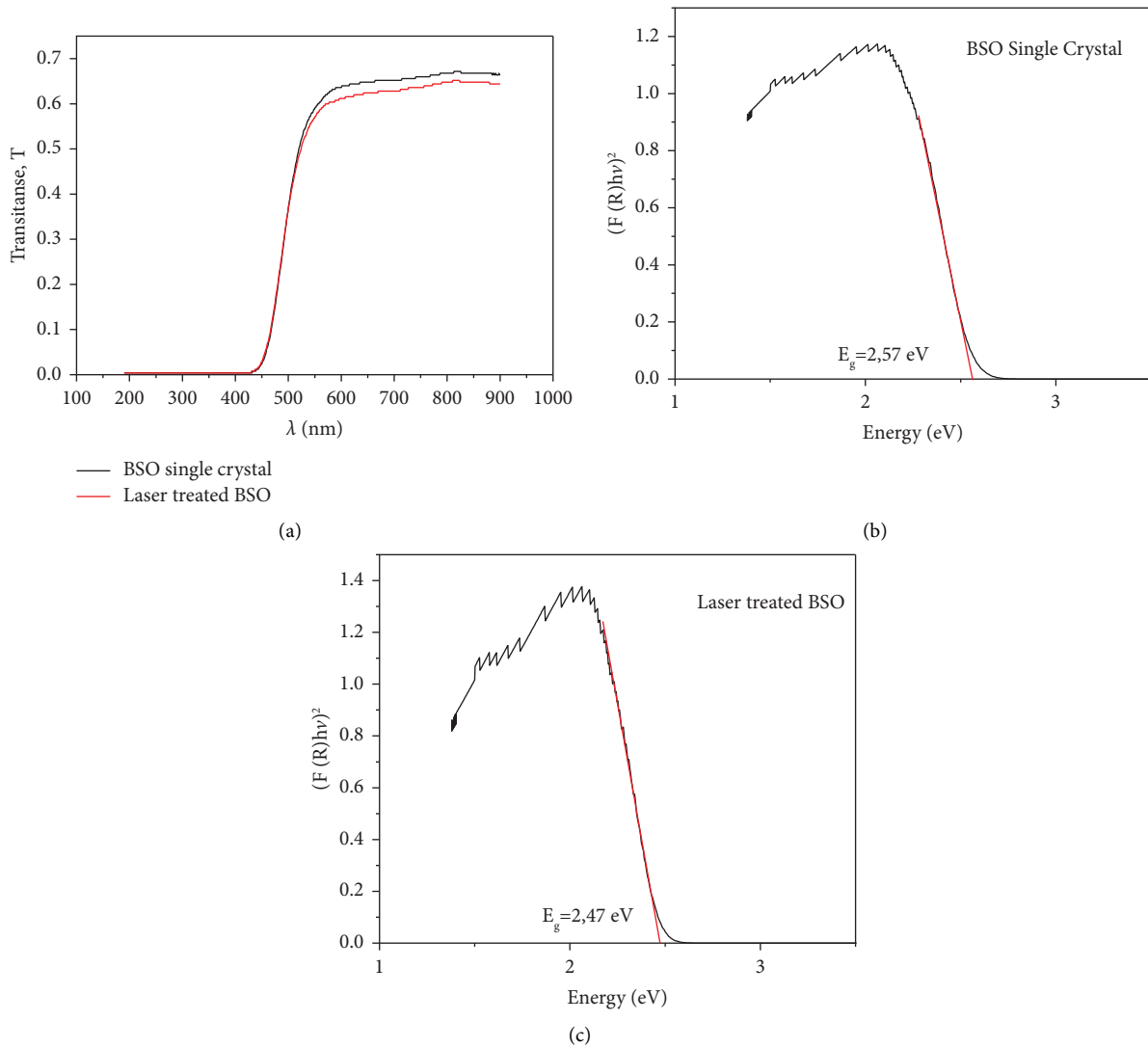


FIGURE 4: (a) UV-Vis transmittance spectra of $\text{Bi}_{12}\text{SiO}_{20}$ single crystal treated by laser power. Kubelka–Munk analysis for laser untreated (b) and treated (c) sample.

transmittance was reduced by about 5%. To determine the value of the energy gap e_g , we used the well-known Kubelka–Munk theory (see for example, [3] and the literature cited there). The results of the analysis are shown in Figures 4(b) and 4(c).

For the untreated BSO single crystal, an energy gap value of 2.57 eV was obtained. This energy is lower than the accepted band gap energy of BSO [3]. This smaller energy was associated with defect centers, as analyzed in [23–25]. A value of 2.47 eV was obtained for the laser-treated sample. Such a simple model cannot provide a complete picture of the modifications made in the sample, but it can indicate a macroscopic change, i.e. a parameter that is in some way its consequence.

3.5. Optical Activity, Faraday Rotation, and Bulk Absorption. Optical activity and Faraday rotation were measured by the free space setup described in [26]. It was noted that significant light scattering in the sample causes cross-talk of the

two channels for the orthogonal polarizations detection. Therefore, birefringent crystal was replaced with a Wollaston prism decoupling the channels but also spoiling evenness of channels losses and forcing the use of two photodiodes. Two channels gain that include optoelectronic conversion efficiencies were equalized by transimpedance resistors.

Background light influence was eliminated using an optical chopper and lock-in amplifier. Laser's polarization instability was converted to light irradiation fluctuations by a polarizing prism mounted after the laser. Δ/Σ normalization method used is insensitive to light irradiation fluctuations but introduces another problem. It was also noted that treated BSO induces more depolarization of light compared to untreated one. This is partially the consequence of nano-objects at the surface of the treated BSO. Contribution of depolarized light is canceled in the subtraction but not in the sum leading to a reduced result for Optical activity and Faraday rotation. It is possible to compensate this effect but only for particular crystal orientation. Instead of that we

averaged the results for three different crystal orientations. Results are presented in Table 1 having in mind scattering while measuring the absorption coefficient lens was used after crystal to focus the light on photodiode. Verdet constant was divided by absorption coefficient to obtain the magneto-optical quality of sample.

4. Discussion

As far as we know, [18] preparation technique which was used ensured maximum quality samples in the limits corresponding to the starting components purity. In the case of $\text{Bi}_{12}\text{GeO}_{20}$ [27], the positive effect of laser radiation on optical characteristics was registered only in materials obtained from starting materials of lower quality. With quality single crystals, it was not possible to improve the optical parameters in this way. This is also the case with $\text{Bi}_{12}\text{SiO}_{20}$, which we treated with a laser, i.e. we have a change of several percentages at maximum laser power.

We can interpret the additional structures from Figures 1(b) and 1(c) as follows. Figure 2 clearly shows nano-objects with dimensions of about 15 nm with very narrow dimensional distributions. It is easy to connect these nano-objects with the new phases from Figure 3, registered for the treated sample. These new phases show their characteristics on Raman spectra as well. First, four polymorphic phases of bismuth-oxide are known: the one stable at the room temperature, orthorhombic $\alpha\text{-Bi}_2\text{O}_3$, and three high-temperature ones: $\beta\text{-}$, $\delta\text{-}$, and $\gamma\text{-Bi}_2\text{O}_3$ [28–30]. Since new structures are visible even at relatively low laser powers, as well as on XRD at room temperature, we can conclude that only the orthorhombic $\alpha\text{-Bi}_2\text{O}_3$ phase is present. In this way, we easily connect the additional structures in the Raman spectra at around 122 cm^{-1} and 456 cm^{-1} with this phase [31]. XRD also registered the Bi_4O_7 phase. This phase has a phonon at 118 cm^{-1} [32], so the presence of the influence of this phase on the phonon registered at 122 cm^{-1} in our experiment is not excluded. The situation is much clearer for the phonon at 486 cm^{-1} . This phonon is associated with Bi-O stretching vibrations in distorted linked BiO_6 units in the previously registered Bi_4O_7 phase [33, 34].

On the other hand, the diversity of SiO_2 -based phases is even greater [35]. However, we think that in our case, SiO_2 clusters have T_d symmetry and corresponding Raman modes at 235 cm^{-1} . Also, experimentally at 463.6 cm^{-1} and theoretically at 461 cm^{-1} , there is a SiO_2 phonon of the same symmetry. Therefore, the origin of the phonon at 456 cm^{-1} cannot be accurately determined, i.e. due to the weak intensity of the experimental result, it is difficult to separate the influence of this phonon from that of $\alpha\text{-Bi}_2\text{O}_3$. This result is in agreement with Ref. [19, 20].

In this way, it is clearly shown that laser heating during the Raman experiment produces nano-objects consisting of bismuth oxide and silicon oxide arranged in a matrix of $\text{Bi}_{12}\text{SiO}_{20}$ single crystal. This structure by its composition can be classified as a nanocomposite because the dispersed phase is in the nanometric size, with the specificity that the nano-object is formed from the same material, or its parts, such as a matrix.

TABLE 1: Optical properties of $\text{Bi}_{12}\text{SiO}_{20}$ single crystal.

	Untreated BSO	Treated BSO
Optical rotatory power (rad/mm)	0.37	0.36
Verdet constant (rad/Tm)	61	58
Absorption coefficient (cm^{-1})	1.03	1.05
Magneto optical quality (rad/T)	0.59	0.55

Our results presented in this paper can be interpreted in at least two ways. First, it can be said that the made modification did not lead to the improvement of the characteristics of the observed material. That is true in principle. But this is practically expected, because the starting material, BSO single crystal, was obtained from ultrapure components, which led to the exceptional optical quality of the sample, as it was the case with the $\text{Bi}_{12}\text{GeO}_{20}$ crystal [18, 27].

However, the modification made led to a partial, but almost controlled, decomposition of the base material. A stable structure was created, which gives the prospect of using nano-objects in robust electronics. Namely, due to their extremely small sizes, nanomaterials (one, two, or three dimensions of less than 100 nm) cannot be used in large scale, particularly as long-bearing materials in engineering applications. For this it has long been a desire to develop bulk composites incorporating these nanomaterials (for example, nanocomposites) to harness their extraordinary properties in bulk applicable materials. Initial ideas and principles are given in [36]. The most important fact is that the characteristics of the nanomaterials are fundamentally different in comparison with the bulk materials [37]. In our opinion, this way of obtaining specific nanocomposites deserves attention.

In addition, in this paper, it is once again shown, this time directly, that during Raman measurement of complex structures and materials, the used laser power should be taken into account. It is very useful to measure Raman spectra with high laser powers. The spectrum is more intense, and the lines are more pronounced. The same applies to the duration of the measurement. However, in those cases, partial decomposition of the observed material or structure may occur, which results in the existence of lines on the spectrum do not belong to the original material, but they are the result of local and partial decomposition. Such results lead to wrong conclusions.

5. Conclusion

High-quality single crystal $\text{Bi}_{12}\text{SiO}_{20}$, with parameters E_g of 2.57 eV, Verdet constant of 61 rad/Tm, and magneto-optical quality of 0.59 rad/T growth by the Czochralski technique. We used 532 nm line of Verdi G optical pumped semiconductor laser, during the Raman experiment, to modify the surface on a $\text{Bi}_{12}\text{SiO}_{20}$ single crystal. By measuring phonon spectra with Raman spectroscopy, starting from the laser power density of $0.7\text{ mW}/\mu\text{m}^2$, and irradiation time greater than 1 s, we have registered new structures at about 122, 235, 456, and 478 cm^{-1} . AFM measurements confirm that the $\text{Bi}_{12}\text{SiO}_{20}$ crystal has decomposed on the surface, and newly formed bismuth oxide and silicon oxide-based

nano-objects in the $\text{Bi}_{12}\text{SiO}_{20}$ matrix was found. This decomposition of $\text{Bi}_{12}\text{SiO}_{20}$ single crystal led to small changes in the electrical and magneto-optical characteristics of the base material. This structure by its composition can be classified as a nanocomposite because the dispersed phase is in the nanometric size, with the specificity that the nano-objects are formed from the same material or its parts, such as a matrix.

Data Availability

Data are available upon reasonable request.

Conflicts of Interest

The authors declare that they have no conflicts of interest.

Acknowledgments

This research was supported by the Science Fund of the Republic of Serbia, Grant no. 7504386, Nano object in own matrix–Self composite–NOOM–SeC.

References

- [1] A. F. Lima, S. A. S. Farias, and M. V. Lalic, “Structural, electronic, optical, and magneto-optical properties of $\text{Bi}_{12}\text{MO}_{20}$ (M = Ti, Ge, Si) sillenite crystals from first principles calculations,” *Journal of Applied Physics*, vol. 110, no. 8, Article ID 083705, 2011.
- [2] D. Hou, X. Hu, Y. Wen et al., “Electrospun sillenite $\text{Bi}_{12}\text{MO}_{20}$ (M = Ti, Ge, Si) nanofibers: general synthesis, band structure, and photocatalytic activity,” *PCCP: Physical Chemistry Chemical Physics*, vol. 15, no. 47, Article ID 20698, 2013.
- [3] M. Isik, S. Delice, N. M. Gasanly, N. H. Darvishov, and V. E. Bagiev, “Temperature-dependent band gap characteristics of $\text{Bi}_{12}\text{SiO}_{20}$ single crystals,” *Journal of Applied Physics*, vol. 126, no. 24, Article ID 245703, 2019.
- [4] V. M. Skorikov, Y. F. Kargin, A. V. Egorysheva, V. V. Volkov, and M. Gospodinov, “Growth of sillenite-structure single crystals,” *Inorganic Materials*, vol. 41, no. S1, pp. S24–S46, 2005.
- [5] R. A. Ganeev, A. I. Ryasnynsky, B. Palpant, and S. Debrus, “Third-order nonlinearities of $\text{Bi}_{12}\text{GeO}_{20}$ crystal measured by nanosecond radiation,” *Journal of Applied Physics*, vol. 97, no. 10, Article ID 104303, 2005.
- [6] M. Itoh, T. Katagiri, H. Mitani, M. Fujita, and Y. Usuki, “Comparative study of excitonic structures and luminescence properties of $\text{Bi}_4\text{Ge}_3\text{O}_{12}$ and $\text{Bi}_{12}\text{GeO}_{20}$,” *Physica Status Solidi (B)*, vol. 245, no. 12, pp. 2733–2736, 2008.
- [7] P. Schaaf, Ed., *Springer Series in Materials Science*, Springer Verlag, Berlin, Germany, 2010.
- [8] M. A. Montealegre, G. Castro, P. Rey, J. L. Arias, P. Vazquez, and M. Gonzalez, “Surface treatments by laser technology,” *Contemporary Materials*, vol. 1, no. 1, pp. 19–30, 2010.
- [9] A. K. Roy, Ed., *Hybrid Atomic-Scale Interface Design for Materials Functionality*, Elsevier, Amsterdam, Netherlands, 2021.
- [10] M. V. Shugaev, C. Wu, O. Armbruster et al., “Fundamentals of ultrafast laser–material interaction,” *MRS Bulletin*, vol. 41, no. 12, pp. 960–968, 2016.
- [11] By M. Cardona, Ed., *Light Scattering of Solids 1*, Springer, Berlin, Germany, 1975.
- [12] B. Hadzic, N. Romcevic, D. Sibera et al., “Laser power influence on Raman spectra of $\text{ZnO}(\text{Co})$ nanoparticles,” *Journal of Physics and Chemistry of Solids*, vol. 91, pp. 80–85, 2016.
- [13] B. Hadzic, B. Vasic, B. Matovic et al., “Influence of laser-induced heating on MnO nanoparticles,” *Journal of Raman Spectroscopy*, vol. 49, no. 5, pp. 817–821, 2018.
- [14] S. Xie, M. P. Rosynek, and H. Lunsford, “Effect of laser heating on the local temperature and composition in Raman spectroscopy: a study of $\text{Ba}(\text{NO}_3)_2$ and BaO_2 decomposition,” *Applied Spectroscopy*, vol. 53, no. 10, pp. 1183–1187, 1999.
- [15] S. Kouteva-Arguirova, T. Z. Arguirov, D. Wolfframm, and J. Reif, “Influence of local heating on micro-Raman spectroscopy of silicon,” *Journal of Applied Physics*, vol. 94, no. 8, p. 4946, 2003.
- [16] N. Romcevic, M. Lekic, A. Kovacevic, N. Paunovic, B. Vasic, and M. Romcevic, “Structural properties of femtosecond laser irradiation induced bismuth oxide-based nano-objects in $\text{Bi}_{12}\text{SiO}_{20}$ (BSO) single crystal,” *Physica E: Low-Dimensional Systems and Nanostructures*, vol. 148, Article ID 115653, 2023.
- [17] *Powder Diffraction File, PDF-2 Database, Announcement of New Database Release*, International Centre for Diffraction Data (ICDD), 2012.
- [18] Z. Z. Lazarevic, P. Mihailovic, S. Kostic et al., “Determination of magneto-optical quality and refractive index of bismuth germanium oxide single crystals grown by Czochralski technique,” *Optical Materials*, vol. 34, no. 11, pp. 1849–1859, 2012.
- [19] S. Venugopalan and A. K. Ramdas, “Raman spectra of bismuth germanium oxide and bismuth silicon oxide,” *Physical Review B: Condensed Matter*, vol. 5, no. 10, pp. 4065–4079, 1972.
- [20] B. Mihailova, M. Gospodinov, and L. Konstantinov, “Raman spectroscopy study of sillenites. I. Comparison between $\text{Bi}_{12}(\text{Si},\text{Mn})\text{O}_{20}$ single crystals,” *Journal of Physics and Chemistry of Solids*, vol. 60, no. 11, pp. 1821–1827, 1999.
- [21] I. F. Vasconcelos, M. A. Pimenta, and A. S. B. Sombra, “Optical properties of $\text{Bi}_{12}\text{SiO}_{20}$ (BSO) and $\text{Bi}_{12}\text{TiO}_{20}$ (BTO) obtained by mechanical alloying,” *Journal of Materials Science*, vol. 36, no. 3, pp. 587–592, 2001.
- [22] J. C. Alonso, R. Diamant, E. Haro-Poniatowski et al., “Raman characterization of $\text{Bi}_{12}\text{SiO}_{20}$ thin films obtained by pulsed laser deposition,” *Applied Surface Science*, vol. 109–110, pp. 359–361, 1997.
- [23] M. Isik, N. Sarigul, and N. M. Gasanly, “Thermoluminescence characteristics of $\text{Bi}_{12}\text{SiO}_{20}$ single crystals,” *Journal of Luminescence*, vol. 224, Article ID 117280, 2020.
- [24] R. Oberschmid, “Absorption centers of $\text{Bi}_{12}\text{GeO}_{20}$ and $\text{Bi}_{12}\text{SiO}_{20}$ crystals,” *Physica Status Solidi (A)*, vol. 89, no. 1, pp. 263–270, 1985.
- [25] M. Isik, S. Delice, H. Nasser, N. M. Gasanly, N. H. Darvishov, and V. E. Bagiev, “Optical characteristics of $\text{Bi}_{12}\text{SiO}_{20}$ single crystals by spectroscopic ellipsometry,” *Materials Science in Semiconductor Processing*, vol. 120, Article ID 105286, 2020.
- [26] P. Mihailovic, S. Petricevic, and J. Radunovic, “Improvements in difference-over-sum normalization method for Faraday effect magnetic field waveforms measurement,” *Journal of Instrumentation*, vol. 1, no. 12, Article ID P12002, 2006.
- [27] A. Kovačević, J. L. Ristić-Djurović, M. Lekić et al., “Influence of femtosecond pulsed laser irradiation on bismuth germanium oxide single crystal properties,” *Materials Research Bulletin*, vol. 83, pp. 284–289, 2016.
- [28] B. Isecke and J. Osterwald, “Gleichgewichtsuntersuchungen am sws,” *Zeitschrift für Physikalische Chemie*, vol. 115, no. 1, pp. 17–24, 1979.

- [29] F. D. Hardcastle and I. E. Wachs, "The molecular structure of bismuth oxide by Raman spectroscopy," *Journal of Solid State Chemistry*, vol. 97, no. 2, pp. 319–331, 1992.
- [30] E. Oniyama and P. G. Wahlbeck, "Phase equilibria in the Bismuth–Oxygen system," *Journal of Physical Chemistry B*, vol. 102, no. 22, pp. 4418–4425, 1998.
- [31] K. Trentelman, "A note on the characterization of bismuth black by Raman microspectroscopy," *Journal of Raman Spectroscopy*, vol. 40, no. 5, pp. 585–589, 2009.
- [32] O. Depablos-Rivera, A. Martinez, and S. E. Rodil, "Interpretation of the Raman spectra of bismuth oxide thin films presenting different crystallographic phases," *Journal of Alloys and Compounds*, vol. 853, Article ID 157245, 2021.
- [33] H. Guan and Y. Feng, "Facile synthesis and purplish blue luminescence of the binary mixed valence compound Bi_4O_7 microcrystals," *Materials Letters*, vol. 143, pp. 269–272, 2015.
- [34] V. Dimitrov, Y. Dimitriev, and A. Montenero, "IR spectra and structure of V_2O_5 , GeO_2 , Bi_2O_3 glasses," *Journal of Non-crystalline Solids*, vol. 180, no. 1, pp. 51–57, 1994.
- [35] C. De La Rocha and D. J. Conley, "Mystical crystals of silica," *Silica Stories*, Springer, Berlin, Germany, 2017.
- [36] Y. Dzenis, "Structural nanocomposites," *Science*, vol. 319, no. 5862, pp. 419–420, 2008.
- [37] T. E. Twardowski, *Introduction to Nanocomposites Material Properties, Processing, Characterization*, Destech Publications, Lancaster, Pa, USA, 2007.